Cell PRESS
Structure
Article

The Mechanisms of HAMP-Mediated Signaling in Transmembrane Receptors

Hedda U. Ferris,[1] Stanislaw Dunin-Horkawicz,[1] Laura García Mondéjar,[2] Michael Hulko,[1] Klaus Hantke,[2] Jörg Martin,[1] Joachim E. Schultz,[2] Kornelius Zeth,[1] Andrei N. Lupas,[1,*] and Murray Coles[1,*]
[1]Department of Protein Evolution, Max-Planck-Institute for Developmental Biology, 72076 Tübingen, Germany
[2]Department of Pharmaceutical Biochemistry, School of Pharmacy, Tübingen University, 72076 Tübingen, Germany
*Correspondence: andrei.lupas@tuebingen.mpg.de (A.N.L.), murray.coles@tuebingen.mpg.de (M.C.)
DOI 10.1016/j.str.2011.01.006

SUMMARY

HAMP domains mediate signal transduction in over 7500 enzyme-coupled receptors represented in all kingdoms of life. The HAMP domain of the putative archaeal receptor Af1503 has a parallel, dimeric, four-helical coiled coil structure, but with unusual core packing, related to canonical packing by concerted axial rotation of the helices. This has led to the gearbox model for signal transduction, whereby the alternate packing modes correspond to signaling states. Here we present structures of a series of Af1503 HAMP variants. We show that substitution of a conserved small side chain within the domain core (A291) for larger residues induces a gradual transition in packing mode, involving both changes in helix rotation and bundle shape, which are most prominent at the C-terminal, output end of the domain. These are correlated with activity and ligand response in vitro and in vivo by incorporating Af1503 HAMP into mycobacterial adenylyl cyclase assay systems.

INTRODUCTION

Prokaryotes sense their environment through an array of dimeric transmembrane receptors. These share a broad modular architecture, with an extracellular, N-terminal sensor coupled to an intracellular, C-terminal effector, which is either an enzyme or regulates an enzyme via adaptor proteins. As sensor and effector lie on opposite sides of the plasma membrane, signal transduction must involve internal conformational changes in the segments linking them. These consist of the membrane-spanning helices followed by a highly variable region, ranging from as little as a short helical extension to multidomain assemblies. Despite this variety, many lines of evidence suggest a common underlying transduction mechanism. Particularly, it has proven possible to create active chimeric receptors by combining modules and linkers from functionally distinct proteins (Appleman and Stewart, 2003; Baumgartner et al., 1994; Kanchan et al., 2010; Utsumi et al., 1989; Weerasuriya et al., 1998). Receptors with simpler linking segments can therefore be used as model systems to study signal transduction in a broader context.

One of the most common domains in linking segments is the HAMP domain, named for its occurrence in histidine kinases, adenylyl cyclases, methyl accepting chemotaxis receptors and phosphatases (Aravind and Ponting, 1999) and present in several thousand proteins either singly or as part of multi-HAMP arrangements, (Aravind and Ponting, 1999; Dunin-Horkawicz and Lupas, 2010a). In transmembrane receptors, the first instance immediately follows the membrane-spanning helices and must be competent in directly accepting and transmitting the transmembrane signal. We solved the first structure of a HAMP domain from the open reading frame Af1503 of *Archaeoglobus fulgidus*, showing a parallel, dimeric, four-helical coiled coil (Hulko et al., 2006). This structure has since been implied for other HAMP domains by cysteine cross-linking studies (Swain and Falke, 2007; Watts et al., 2008) and most recently confirmed by crystallography (Airola et al., 2010). As expected for a coiled coil, HAMP displays a seven-residue sequence pattern (the heptad repeat), whose positions are labeled *a–g* and where hydrophobic residues occupy positions *a* and *d*. However, the Af1503 HAMP domain shows an unexpected packing mode (complementary *x-da*), related to the canonical *knobs-into-holes* packing of coiled coils by a concerted axial rotation of all four helices (Figure 1A). This prompted us to introduce the gearbox model for transmembrane signaling, whereby an incoming signal initiates helix rotation around an axis perpendicular to the membrane, causing a transition between these packing modes (Hulko et al., 2006).

To test this model we created HAMP variants designed to induce the proposed packing transition, targeting a conserved, unusually small residue within the domain core (A291) for substitution. Large, hydrophobic residues are far more common in these positions in canonical coiled coils, and we reasoned that such residues would favor *knobs-into-holes* packing, in line with phenotypes observed for equivalent substitutions in two histidine kinases: EnvZ (Tokishita et al., 1992) and NarX (Appleman and Stewart, 2003). Ensuing functional studies of Af1503 chimeras showed a clear correlation between activity and side chain volume at this position, most strikingly in a mycobacterial adenylyl cyclase system (Figure 1B) (Hulko et al., 2006). However, we could not confirm this structurally, as the main variant we studied, A291V, could not be resolved to a single

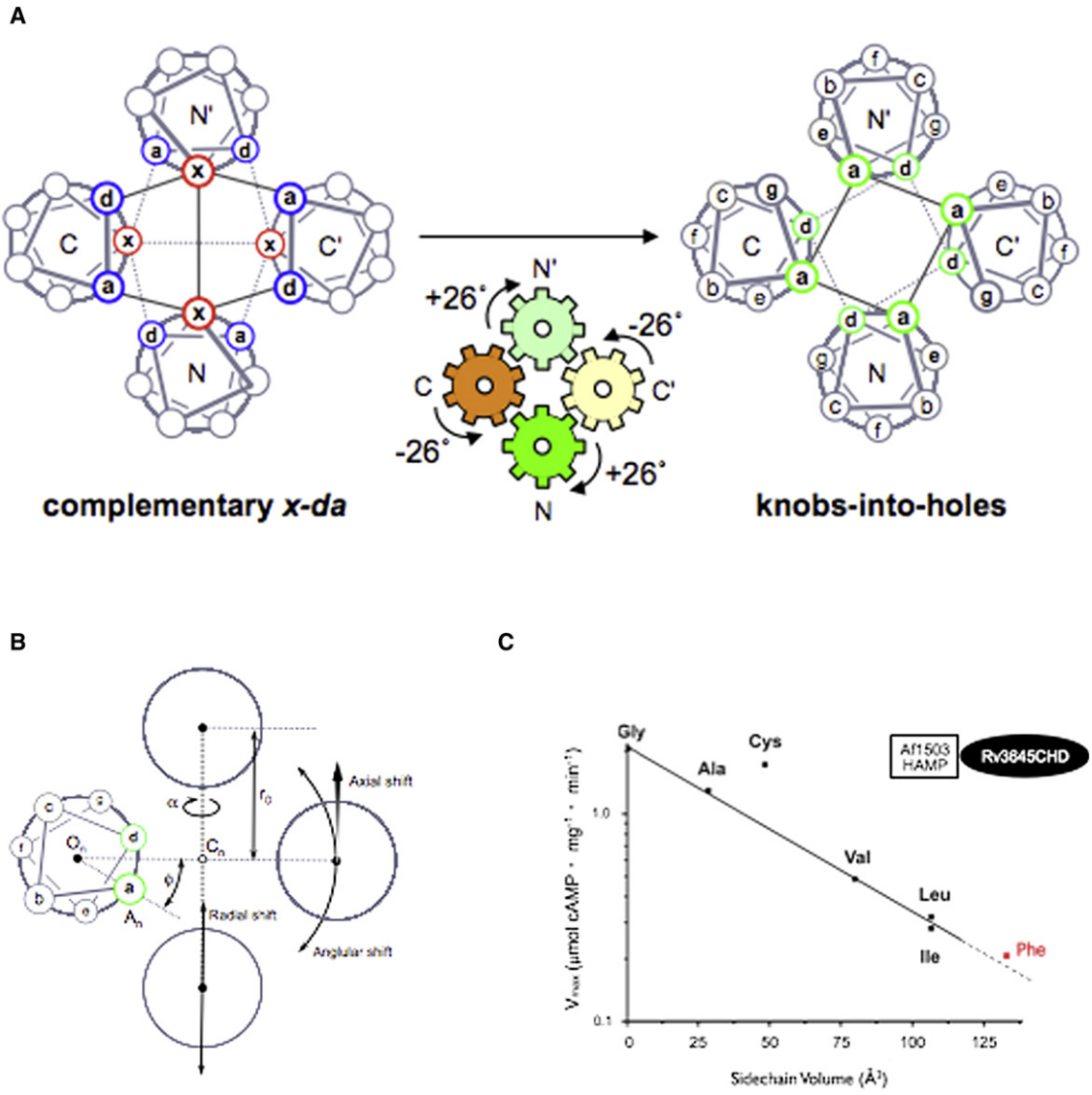

Figure 1. The Gearbox Model of HAMP-Mediated Signaling

(A) Schematic representations of complementary *x-da* (left) and *knobs-into-holes* packing (right). Helical wheel diagrams are shown (N terminus toward the viewer), with core residues in bold face. Solid and dashed lines join interacting residues of the first and second core layers, respectively. Complementary *x-da* packing combines two residues in *x*-geometry (pointing toward each other across the bundle axis; red) with four residues in *da*-geometry (forming a ring flanking the bundle core; blue). Each helix alternates in providing one *x*- and two *da*-residues to the core in successive layers. In canonical *knobs-into-holes* geometry (left), each helix provides one residue per layer to the core, with each in the same geometry (green). The two packing modes interconvert by rotating adjacent helices by 26° in opposite directions, as illustrated by the cogwheel diagram.

(B) Coiled-coil parameters for a four-helix bundle. The axis of each helix (O_n) is shown as a black circle, whereas the axis of the bundle (C_n) is white. The circles of the helical wheel diagram represent the C_α positions (A_n) for each residue of a heptad repeat. The rotation state is expressed as the Crick angle (ϕ), defined as the angle C_n-O_n-A_n, as shown for position *a*. The supercoil crossing angle (that between the bundle axis and each helix axis) is denoted α, whereas the bundle radius is r_0. The program samCC (Dunin-Horkawicz and Lupas, 2010a) reports parameters for each residue in each helix, after correcting for distortions from ideal bundle shape, i.e., angular, radial and axial shifts.

(C) In vitro adenylyl cyclase activities of Af1503 HAMP-Rv3645CHD chimeras. Activities are plotted as a function of side chain volume at HAMP position 291. The black points are as reported previously (Hulko et al., 2006), the red point shows extension of the series to phenylalanine. The linear fit includes all data points except A291C.

structure due to internal dynamics (Hulko et al., 2006). This observation was at least consistent with a transition between packing modes, and we saw the potential to extend the series to larger side chains and solve structures for the range of obtained variants. We show that increasing side chain size at position 291 induces a gradual change in the core packing of HAMP and correlate this with effector output in adenylyl cyclase assay systems in vitro and in vivo.

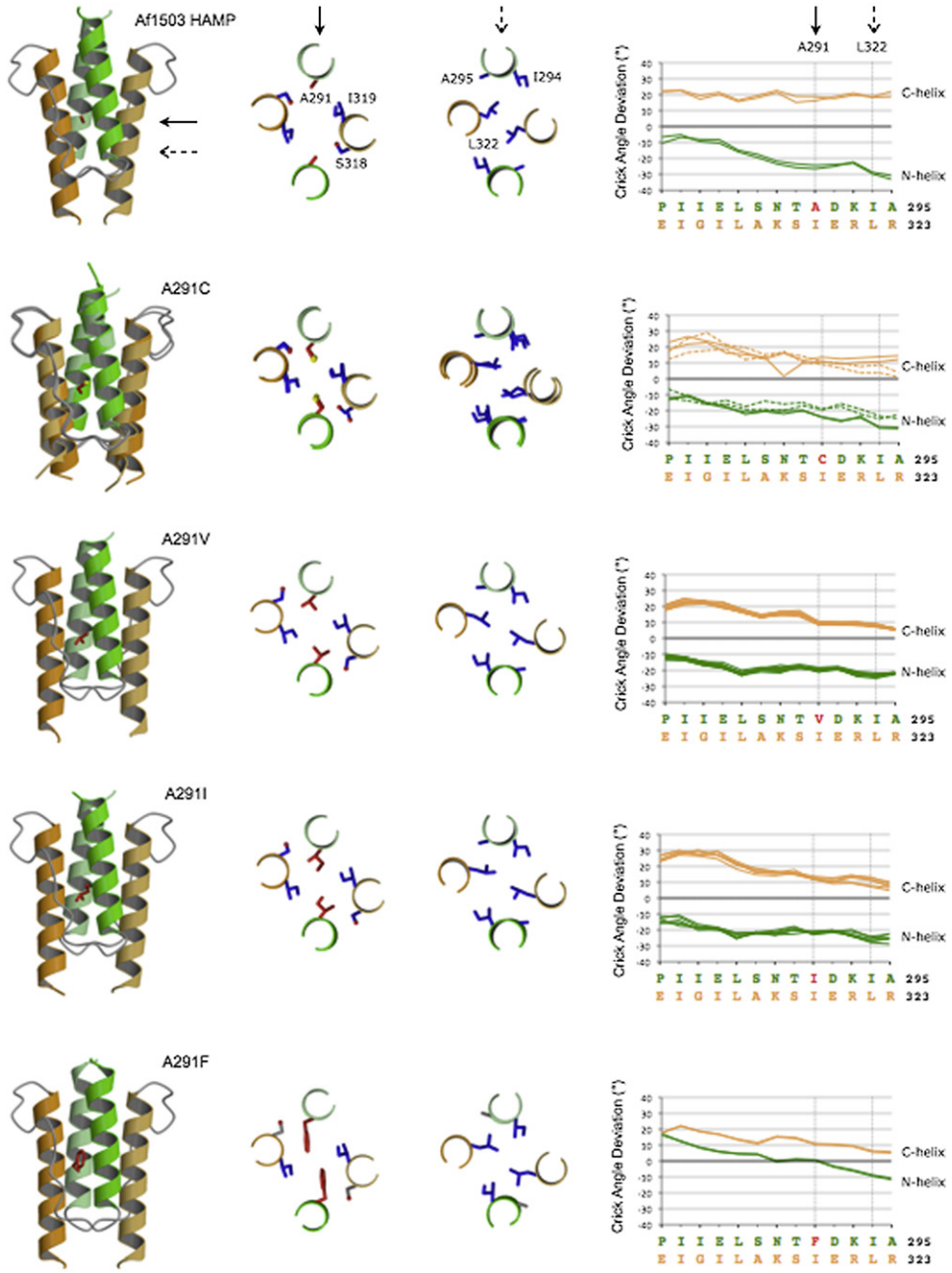

Figure 2. Structures of Isolated Af1503 HAMP A291 Variants

Wild-type and A291F are solution structures and A291C, V and I are crystal structures (see Table S1 and Table S2 for structural statistics). For A291C, both dimers within the asymmetric unit are shown superimposed. In each row, the left panel shows a secondary structure cartoon, with N-terminal helices green and C-terminal helices orange, and monomers distinguished by light and dark shading. The central panel shows two layers viewed from the N-terminal end: that involving the substituted position (left) and the last core layer (right). The positions of these layers are marked by arrows on the wild-type structure. The right panel plots the rotation state for each residue relative to the expectation for idealized *knobs-into-holes* packing (plotted for all dimers in the asymmetric unit for the crystal structures).

RESULTS AND DISCUSSION

Structures of Af1503 HAMP Variants

To explore the effect of A291 substitution on the structures of isolated domains, we selected three variants from our existing series. In addition we extended the series to phenylalanine, which proved to be the largest side chain tolerated in this position (a tryptophan variant was unfolded). We obtained crystal structures for the A291C, V and I variants, and both crystal and nuclear magnetic resonance (NMR) structures for A291F (Figure 2). We also refined the original solution structure of wild-type domain using our methods based on back-calculation

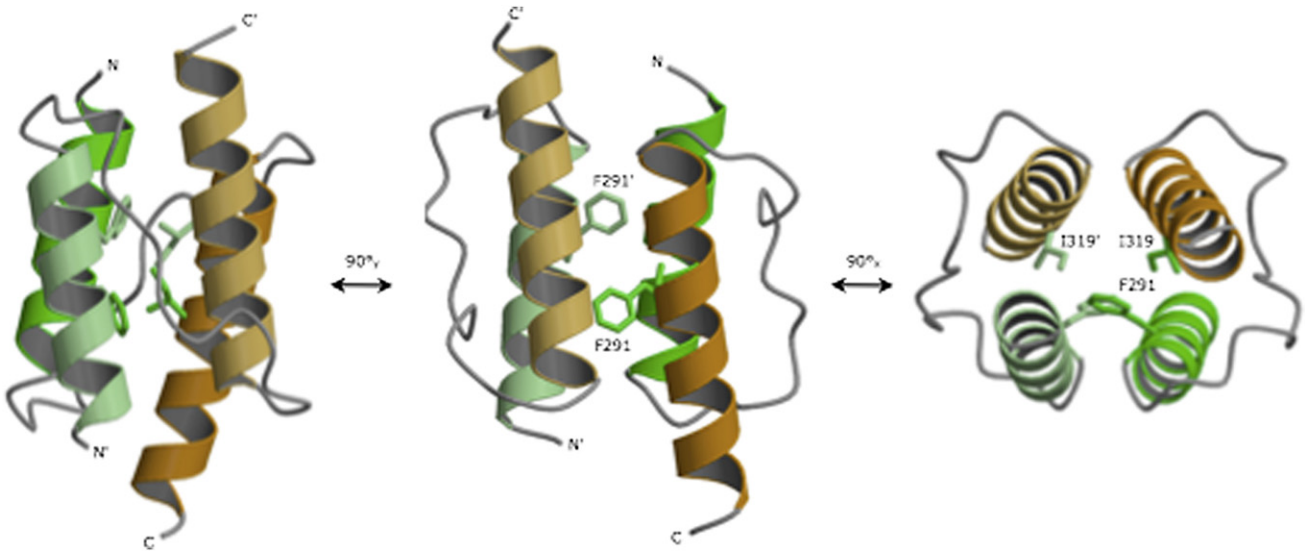

Figure 3. The Af1503 HAMP (A291F) Crystal Structure Forms an Antiparallel Dimer

Secondary structure cartoons are shown, colored as in Figure 1. The two residues shown as sticks (the substituted phenylalanine, F291 and I319) form a single layer in the parallel structure. An equal mixture of this antiparallel dimer and the parallel dimer shown in Figure 2 are present in solution. Expectation spectra back-calculated from both forms match the experimental NOESY spectra very well (Figure S1).

of expectation nuclear Overhauser enhancement spectroscopy (NOESY) spectra (see Experimental Procedures), assigning several new contacts, particularly toward the C terminus of the domain. To analyze these structures quantitatively, we developed the program samCC, which calculates a range of structural parameters for square four-helix bundles (Dunin-Horkawicz and Lupas, 2010b). The helix rotation state of each structure relative to expectation values for canonical *knobs-into-holes* packing is shown in Figure 2.

For the wild-type domain, the rotation state at the center of the bundle (the N289/K317 layer in the plots) is −23°/+22° (referring to the average rotation of the N- and C-helices, respectively), corresponding to the ±26° rotation originally proposed as the hallmark of complementary *x-da* packing. In the A291C, V and I variants, the N- and C-helices are also rotated away from canonical packing, but to a lesser extent. These structures have average rotation states at their respective bundle centers of –19°/+16°, –20°/+15°, and –21°/+16°. Although we had not originally anticipated this possibility, benchmarking samCC on coiled coils of known structure showed that a continuum of rotation states is indeed possible between canonical *knobs-into-holes* packing (±0°) and complementary *x-da* (±26°) (Dunin-Horkawicz and Lupas, 2010b).

Increasing the side chain size at position 291 to phenylalanine had unexpected structural consequences. The crystal structure of the A291F variant also shows a four-helical bundle of wild-type-like monomers, but these assume a nonphysiological antiparallel orientation, presumably due to steric tension introduced by the large aromatic side chains (Figure 3). In solution, this variant is an almost equal mixture of antiparallel and parallel dimeric forms. Whereas the antiparallel form corresponds to the one in the crystal structure, the parallel form could be solved separately and is presented in Figure 2 (see also Figures S1 and S2 available online). Increased side chain size had the predicted effect on its packing mode, which is close to canonical *knobs-into-holes* (rotation state for the bundle center 0°/15°).

Although we observe a graded change in rotation states as a function of side chain size at position 291, we see a more polarized change in the shape of the four-helix bundle (Figure 4). The wild-type helices are angled with respect to each other, and the layers have rhombic cross-sections toward the helix termini. In contrast, the C-helices of the A291V and I variants are close to parallel, resulting in approximately square cross-sections for the lower layers (Figures 2 and 4). In A291C, one dimer of the asymmetric unit is more similar to wild-type and the second more similar to the other variants. For A291F, the bundle shape resembles that of A291V and A291I, but in this case the N-helices are also close to parallel, and the layers have square cross-sections throughout.

The variants also show differences in helix periodicity. For most helices, the plots shown in Figure 2 have a negative slope, indicating that they depart from the ideal heptad periodicity of the reference structure (7 residues over 2 turns = 3.5), tending toward the value expected for straight helices (18/5 = 3.6). This includes all variant structures, meaning that the plots for their N- and C-helices are parallel and maintain a constant difference in rotation state throughout. The situation is different for the wild-type, where the C-helices have periodicity close to 3.5. This results in an increasing difference in rotation state between the N- and C-helices toward their C-termini.

In comparing the different structures, we find that their rotation states fall roughly into three groups, wild-type, A291C/V/I, and A291F. This is similar for bundle shape, with the difference that one form of A291C groups with wild-type. With regard to helix periodicity, the wild-type shows a large difference between the N- and C-helices, whereas all others have similar values

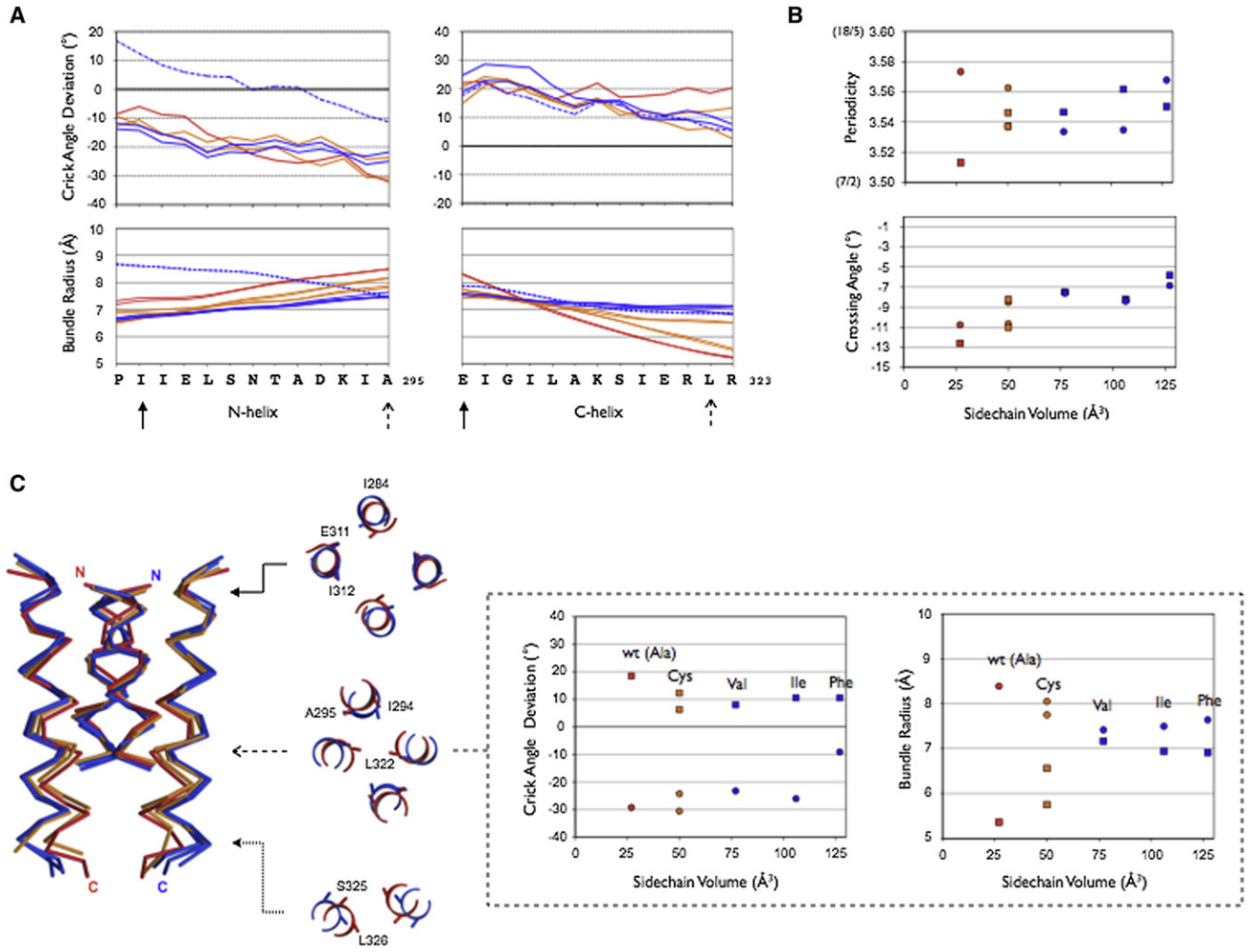

Figure 4. Effects of Af1503 HAMP A291 Substitution

In all panels wild-type is shown in red, A291C in orange. and A291V/I/F in blue. Solid and dashed arrows mark the same positions in (A) and (C). N-helices are shown as circles and C-helices as squares in (B) and (C).

(A) Plots of rotation state and bundle radius for the N- and C-helices. Both dimers in the A291C asymmetric unit are plotted, as they differ considerably. The A291F variant is shown with dotted lines.

(B) Plots of helix periodicity and crossing angle versus side chain size at position 291.

(C) Superimposition of all Af1503 HAMP structures over all helical residues. Structures are clustered into two groups based on side chain size at position 291, with each group containing one of the two A291C structures. The three layers shown in cross section compare wild-type with A291F, illustrating differences in bundle shape and rotation state. The plots show the rotation state and bundle radius for the last HAMP core layer versus side chain size at position 291. Transverse ^{15}N relaxation times for the A291F variant show values intermediate between those previously reported for wild-type and A291V (Hulko et al., 2006), indicating moderate internal motions on millisecond timescales (see Figure S2).

intermediate between 7/2 and 18/5 (Figure 4B). These structural parameters combine to determine the super-coil crossing angles (between the helix and bundle axes) of the different HAMP forms; these show a fairly continuous correlation with side chain size at position 291 (Figure 4B). Thus increases in side chain size progressively bias the structure toward *knobs-into-holes* packing, but this is not achieved purely by axial helix rotation. Rather, a number of additional, correlated changes contribute to this transition. It is notable that the N-termini of all C-helices are similar in terms of both rotation state and bundle radius (Figure 4A). Thus the packing transition projects the largest differences toward the C terminus, representing the output of the domain.

Functional Assays of Af1503 HAMP-Adenylyl Cyclase Chimeras

Our original functional studies on Af1503 HAMP included a chimeric mycobacterial adenylyl cyclase system, i.e., N-terminal fusion of the domain to the cyclase-homology domain (CHD) of Rv3645 (Hulko et al., 2006). We extended this system to include the A291F variant, which has the lowest cyclase activity of the series (Figure 1B, red data point), in line with its *knobs-into-holes* structure. This demonstrates that rational alterations to the HAMP domain based on the gearbox model result in consistent phenotypes.

To test whether the A291 variants were also competent in signal transduction in this system, we further developed the

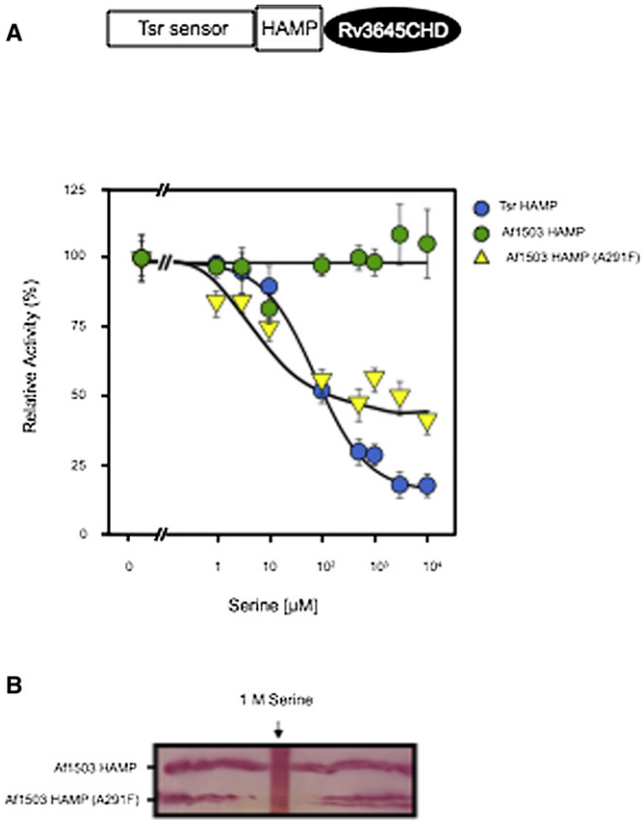

Figure 5. Chimeric Adenylyl Cyclase Assay Systems

(A) In vitro activity in Tsr sensor-HAMP-CHD chimeras. The plots show the serine response of constructs containing Tsr HAMP (responsive; blue points), Af1503 HAMP (insensitive; green points) and Af1503 HAMP A291F (responsive; yellow points). Values are means ± standard error of mean of two to four data points. One hundred percent activity was 18.4, 19.0, and 8.2 nmol cAMP/min/mg for Tsr HAMP, Af1503 HAMP, and Af1503 HAMP (A291F), respectively.

(B) MacConkey maltose agar plate assays demonstrate the restoration of serine response in the A291F variant in vivo; production of cAMP (indicated by red coloring of the plate) is downregulated in the vicinity of the serine soaked strip.

assay to allow us to assess ligand response. We created chimeric receptors by N-terminally fusing the sensor domain and transmembrane region from the *Escherichia coli* serine chemoreceptor, Tsr, to the HAMP-CHD constructs. An equivalent construct containing Tsr HAMP actively produces cAMP and is regulated by serine (82% inhibition at 10 mM serine) (Kanchan et al., 2010). In contrast, the construct containing wild-type Af1503 HAMP is constitutively active and unresponsive to serine over the concentration range tested (Figure 5A). Regulation by serine is gained by the A291F variant, whose cAMP production is inhibited by 58% at 10 mM serine. Note that the serine response of the chimeras is opposite to that of native Tsr, in that increasing serine concentration downregulates cyclase activity, whereas it upregulates the activity of the Tsr-linked kinase. This result is supported by in vivo MacConkey plate assays. Cells expressing the wild-type protein produce sufficient cAMP to activate maltose fermentation, the acidic byproducts of which color the plate pH indicator red. For the A291F variant, a loss of color is observed in the vicinity of a serine soaked-strip, indicating that cAMP production has been suppressed (Figure 5B). Thus, both in vitro and in vivo, Af1503 HAMP constitutively activates the cyclase and regulation is only achieved by increasing the side chain size at position 291.

Mechanism of Signal Transduction

Our series of variants was designed to induce a transition from the complementary *x-da* packing of the wild-type domain toward canonical *knobs-into-holes* packing. Structural analysis confirms this transition, showing that it involves both changes in helix rotation and bundle shape. Our functional assays correlate these packing modes with consistent phenotypes.

Although we could solve solution structures at the end points of the series, crystal structures were required for the intermediate variants; in our previous studies, the A291V variant could not be resolved to a single structure due to internal motions (Hulko et al., 2006). The effect of substitution at position 291 is therefore best viewed as decreasing the threshold for the transition in packing modes. In line with this, substitution for larger side chains in the Tsr-HAMP-CHD constructs does not inactivate the receptors, but makes them responsive to ligand input. We therefore interpret the crystal structures as snapshots of the packing transition.

In the last year the number of published HAMP structures has risen from one to four with the publication of a single structure; that of a tri-HAMP array from Aer2, a soluble aerotaxis receptor from *Pseudomonas aeruginosa* (3LNR; Airola et al., 2010). All three HAMP domains in this structure conform to the general architecture established by Af1503 HAMP. The first and third domains (HAMP1 and HAMP3) also resemble Af1503 HAMP in their overall form: the helices of both are angled such that the N-helices diverge toward the C terminus, whereas the C-helices converge, and both have heptad periodicities with rotation states at their bundle centers of $-11°/+20°$ and $-13°/+21°$, respectively. HAMP2, however, is considerably different: its N-helices diverge and C-helices converge toward the C terminus, and it has an 18/5 residue periodicity with a rotation state of $-4°/+15°$ at the bundle center. Most conspicuous is the invasion of a conserved, hydrophobic residue from the interhelical connector (I88 in Aer2, equivalent to V303 in Af1503) into the domain core.

The structural differences of HAMP2 make it tempting to propose this as the alternate signaling state (Airola et al., 2010; Parkinson, 2010). Although attractive in the context of Aer2-mediated aerotaxis, several considerations caution against extending this to transmembrane signaling. Our bioinformatics analysis places all three Aer2 HAMPs into small, divergent clusters, which are well separated from the central super-cluster of canonical HAMPs. Domains from these divergent clusters do not occur in the context of the membrane and lack the network of coevolving residues implicated in accepting the transmembrane signal (Dunin-Horkawicz and Lupas, 2010a). In contrast, all HAMP domains that have been recombined within functional chimeric receptors, including Af1503 HAMP, belong to the canonical super-cluster and contain the relevant residue network. Indeed, there is no evidence that the Aer2 tri-HAMP module could relay transmembrane signals given that it has never been recombined into a functional transmembrane

receptor and aerotaxis receptors are known to accept an intracellular signal.

Our structures demonstrate that transmembrane signaling can be explained without invoking the larger-scale structural changes involved in converting the Af1503 HAMP topology to that of Aer2 HAMP2. The more subtle changes in packing modes we observe suffice to deliver changes in both helix rotation and bundle radius to downstream effector domains. How these are interpreted to produce an output will require studies of larger constructs combining HAMP with downstream domains. We consider it likely that each effector domain type will be found to respond to different aspects of the signal, and each in its own way.

EXPERIMENTAL PROCEDURES

Protein Preparation and Assays

A detailed list of bacterial strains and constructs is given in the Supplemental Experimental Procedures. Isolated Af1503 HAMP constructs and the chimera between Afl503 HAMP (A291F) and the mycobacterial adenylyl cyclase Rv3645 were created as described previously (Hulko et al., 2006).

Constructs for the chimeric Tsr-adenylyl cyclase assay system (Tsr_{1-268}-$Rv3645CHD_{331-549}$) were made as previously published (Kanchan et al., 2010), but with the wild-type and A291F variant Af1503 $HAMP_{278-331}$ coding sequences each incorporated in the place of the Tsr HAMP coding sequence. AC activity was determined at 37°C for 10 min in 100 μl (Salomon et al., 1974). Standard reactions contained 50 mM Tris/HCl, pH 7.5, 22% glycerol, 3 mM $MnCl_2$, 200 μM [α-^{32}P]adenosine triphosphate (ATP) (Rv3645) or 750 μM [α-^{32}P]ATP (CyaG), and 2 mM [2,8-^{3}H]cAMP to monitor yield during product purification. Creatine kinase and creatine phosphate were used as an ATP regenerating system. Cyclic adenosine monophosphate (AMP) production was ascertained in vivo via MacConkey maltose agar plates as previously published (Kanchan et al., 2010). As an internal control, Rv3645CHD holoenzyme exposed to the same concentration range of serine was found to have an unaffected basal activity (data not shown).

NMR Structure Determination

Spectra of Af1503 HAMP A291F were recorded at 308 K on Bruker spectrometers at 600 or 900 MHz. Backbone sequential assignments were made using 3D-^{15}N-HSQC-NOESY and 3D-NNH-NOESY spectra to trace the strong HN_i-HN_{i+1} contacts in helical segments, and confirmed using HNCA experiments. The remaining ^{13}C assignments were completed using CBCA(CO)NH, HNCO, 3D-CC(CO)NH-TOCSY and 3D-CCH-TOCSY spectra. An HNHB spectrum was acquired to assist in rotamer assignments.

Distance data were derived from 3D-^{15}N-HSQC-NOESY and 3D-NNH-NOESY spectra on a ^{15}N-labeled sample, and 3D-^{13}C-HSQC-NOESY and 3D-CCH- and 3D-CNH-NOESY spectra (Diercks et al., 1999) on a ^{15}N,^{13}C-labeled sample. Aromatic contacts were observed in ^{15}N-filtered 2D-NOESY spectra and intermolecular contacts in ^{14}N,^{12}C- filtered/^{13}C-edited 2D-NOESY spectrum on a mixed double labeled/unlabeled sample. Where possible, contacts identified in the filtered/edited experiments were quantified in other spectra.

Structural restraints were compiled using a protocol aimed at high local accuracy using expectation NOESY spectra to test local conformational hypotheses (in-house software). Chemical shift similarity searches using TALOS (Cornilescu et al., 1999), were used to generate hypotheses for backbone conformations, whereas side-chain rotamers ($\chi1/\chi2$ for leucine and isoleucine, $\chi1$ for all others) were searched exhaustively. Conformations identified in this manner were applied via dihedral restraints, using the TALOS-derived tolerances for backbone and ±30° for side chains. Further NOE contacts were assigned iteratively using back-calculation of expectation NOESY spectra from preliminary structures. Quantification of NOESY data and calculation protocols were as previously described (Hulko et al., 2006), except that refinement was carried out without restraining the symmetry of the dimer. Statistics for all structures are presented in Table S1.

X-Ray Crystallography

Hanging drops were prepared by incubating 1 μl of HAMP construct and 1 μl of reservoir solution at 293 K. Crystallization screens (Hampton, QIAGEN, Emerald Biosystems) typically tested 400–600 conditions. The drops were analyzed by the Rock Imager 54 system (Formulatrix, Waltham).

X-ray data were collected at beamlines PXI or PXII at the Swiss Light Source (Villigen, Switzerland). Diffraction experiments were conducted at 100 K and images were recorded on a 165 or 225 mm MARCCD camera (MAR Research, Norderstedt). Data were indexed, integrated and scaled by the programs XDS and XSCALE (Kabsch, 1993).

Structures were solved by molecular replacement starting from the Af1503 HAMP solution structure using MOLREP (Vagin and Teplyakov, 1997). Model building and refinement of all structures was performed in CCP4i (Potterton et al., 2003) and Coot (Emsley and Cowtan, 2004). Crystallization conditions, crystal preparation, and structure statistics are summarized in Table S2.

ACCESSION NUMBERS

Crystal structures of Af1503 HAMP A291C, A291F, A291V, and A291I and the solution structure of A291F have been deposited in the Protein Data Bank (accession numbers 2Y0Q, 2Y0T, 2Y20, 2Y21, and 2L7I respectively). The solution structure for wild-type has been updated with the refined coordinates (2L7H). Chemical shifts have been deposited in the Biological Magnetic Resonance Data Bank.

SUPPLEMENTAL INFORMATION

Supplemental Information includes Supplemental Experimental Procedures, two figures, and two tables and can be found with this article online at doi:10.1016/j.str.2011.01.006.

ACKNOWLEDGMENTS

We thank Franziska Berndt and Anita Schultz for help with the initial Af1503 constructs, The NMR structures were determined by M.C. and the crystal structures by K.Z. Protein biochemistry was by H.U.F., M.H., and J.M. The adenylyl cyclase studies by L.G.M., K.H., and J.E.S. Structure analysis and molecular modeling were by M.C., S.D-H., and A.N.L. The manuscript was written by M.C., A.N.L., and H.U.F. This work was supported by a research fellowship from the Alexander von Humboldt Foundation to H.U.F, a grant of the Deutsche Forschungsgemeinschaft (SFB766/B8) to J.E.S. and institutional funds of the Max Planck Society.

Received: September 9, 2010
Revised: December 6, 2010
Accepted: January 6, 2011
Published: March 8, 2011

REFERENCES

Airola, M.V., Watts, K.J., Bilwes, A.M., and Crane, B.R. (2010). Structure of concatenated HAMP domains provides a mechanism for signal transduction. Structure *18*, 436–448.

Appleman, J.A., and Stewart, V. (2003). Mutational analysis of a conserved signal-transducing element: the HAMP linker of the Escherichia coli nitrate sensor NarX. J. Bacteriol. *185*, 89–97.

Aravind, L., and Ponting, C.P. (1999). The cytoplasmic helical linker domain of receptor histidine kinase and methyl-accepting proteins is common to many prokaryotic signalling proteins. FEMS Microbiol. Lett. *176*, 111–116.

Baumgartner, J.W., Kim, C., Brissette, R.E., Inouye, M., Park, C., and Hazelbauer, G.L. (1994). Transmembrane signalling by a hybrid protein: communication from the domain of chemoreceptor Trg that recognizes sugar-binding proteins to the kinase/phosphatase domain of osmosensor EnvZ. J. Bacteriol. *176*, 1157–1163.

Cornilescu, G., Delaglio, F., and Bax, A. (1999). Protein backbone angle restraints from searching a database for chemical shift and sequence homology. J. Biomol. NMR *13*, 289–302.

Diercks, T., Coles, M., and Kessler, H. (1999). An efficient strategy for assignment of cross-peaks in 3D heteronuclear NOESY experiments. J. Biomol. NMR *15*, 177–180.

Dunin-Horkawicz, S., and Lupas, A.N. (2010a). Comprehensive analysis of HAMP domains: Implications for transmembrane signal transduction. J. Mol. Biol. *397*, 1156–1174.

Dunin-Horkawicz, S., and Lupas, A.N. (2010b). Measuring the conformational space of square four-helical bundles with the program samCC. J. Struct. Biol. *170*, 226–235.

Emsley, P., and Cowtan, K. (2004). Coot: model-building tools for molecular graphics. Acta Crystallogr. D Biol. Crystallogr. *60*, 2126–2132.

Hulko, M., Berndt, F., Gruber, M., Linder, J.U., Truffault, V., Schultz, A., Martin, J., Schultz, J.E., Lupas, A.N., and Coles, M. (2006). The HAMP domain structure implies helix rotation in transmembrane signaling. Cell *126*, 929–940.

Kabsch, A. (1993). Automatic processing of rotation diffraction data from crystals of initially unknown symmetry and cell constants. J. Appl. Cryst. *26*, 795–800.

Kanchan, K., Linder, J., Winkler, K., Hantke, K., Schultz, A., and Schultz, J.E. (2010). Transmembrane signaling in chimeras of the Escherichia coli aspartate and serine chemotaxis receptors and bacterial class III adenylyl cyclases. J. Biol. Chem. *285*, 2090–2099.

Parkinson, J.S. (2010). Signaling mechanisms of HAMP domains in chemoreceptors and sensor kinases. Annu. Rev. Microbiol. *64*, 101–122.

Potterton, E., Briggs, P., Turkenburg, M., and Dodson, E. (2003). A graphical user interface to the CCP4 program suite. Acta Crystallogr. D Biol. Crystallogr. *59*, 1131–1137.

Swain, K.E., and Falke, J.J. (2007). Structure of the conserved HAMP domain in an intact, membrane-bound chemoreceptor: a disulfide mapping study. Biochemistry *46*, 13684–13695.

Salomon, Y., Londos, C., and Rodbell, M. (1974). Highly sensitive adenylate cyclase assay. Anal. Biochem. *58*, 541–548.

Tokishita, S., Kojima, A., and Mizuno, T. (1992). Transmembrane signal transduction and osmoregulation in Escherichia coli: functional importance of the transmembrane regions of membrane-located protein kinase EnvZ. J. Biochem. (Tokyo) *111*, 707–713.

Utsumi, R., Brissette, R.E., Rampersaud, A., Forst, S.A., Oosawa, K., and Inouye, M. (1989). Activation of bacterial porin gene expression by a chimeric signal transducer in response to aspartate. Science *245*, 1246–1249.

Vagin, A., and Teplyakov, A. (1997). MOLREP: an automated program for molecular replacement. J. Appl. Cryst. *30*, 1022–1025.

Watts, K.J., Johnson, M.S., and Taylor, B.L. (2008). Structure-function relationships in the HAMP and proximal signaling domains of the aerotaxis receptor Aer. J. Bacteriol. *190*, 2118–2127.

Weerasuriya, S., Schneider, B.M., and Manson, M.D. (1998). Chimeric chemoreceptors in Escherichia coli: signaling properties of Tar-Tap and Tap-Tar hybrids. J. Bacteriol. *180*, 914–920.